Lab Automation Drones for Mobile Manipulation in High Throughput Systems

Dongbin Kim
Drones and Autonomous Systems Lab
University of Nevada, Las Vegas (UNLV), USA
Email: dongbin.kim@unlv.edu

Paul Y. Oh
Drones and Autonomous Systems Lab
University of Nevada, Las Vegas (UNLV), USA
Email : paul.oh@unlv.edu

Fig. 1. High Throughput Screening Laboratoy

Fig. 2. Mobile manipulator for HTS proof-of-concept design

***Abstract*—In this paper, a lab automation drone notional concept is introduced. Here, a robotic limb is attached to a robotic rotorcraft. The limb's gripper allows the unmanned aerial vehicle to dexterously manipulate objects such as micro-arrays and test tubes often used in high throughput systems (HTS). The resulting drone could augment existing HTS operations. The 6 degree-of-freedom (DOF) arm and gripper design are presented. Test-and-evaluation approach and results are also given.**

I. Introduction

In lab automation, there is a wide range of robots (Fig. 1). Robots are employed to accelerate sample handling, such as in high throughput screening (HTS), in which manipulators and transfer lines rapidly manipulate micro-plates amongst numerous test stations. The net result is that a typical HTS system can handle over 500,000 samples a week. In the age of big data, higher throughput means faster pharmaceutical development and hence quicker patent registrations and earlier market penetration [1] [2].

HTS systems are often custom-tailored to maximize throughput. However, once configured, they are not easily changed. This is important because as new tests emerge, older HTS systems cannot easily perform them. The National Institutes of Health (NIH) in the United States are looking at the potential of lab automation drones to add flexibility to existing HTS systems. The notion has merit; aerial manipulation research is an active area and micro-plates are relatively easy to robotically lift and orient. Issues like ground effect, limited battery life, and obstacle avoidance are indeed relevant to lab automation but also remain open research topics. The *critical gap* in a lab automation drone appears to be the lack of aerial manipulation arms and grippers. This paper thus presents a 6-DOF parallel mechanism arm with a sensorized parallel jaw gripper (see Fig. 2). Section II describes related work; Section III describes hardware and software components; Section IV showcases testing-and-evaluation results; and Section V concludes and discusses future work.

II. Related Work

Today's state-of-the-art HTS feature many high-precision 6-DOF robot manipulators. Examples include the Staubli RX160, and the Tecan RoMa and Pick-and-Place (PnP) arms to load and place micro-plates from one instrument to another [3] [4]. Such robots employ parallel jaw grippers to gently and precisely position and orient micro-plates.

The ability for aerial vehicles to manipulate or carry objects that they encounter has greatly expanded the types of missions achievable by unmanned aerial systems. High degree of freedom (DOF) robots with dexterous arms have been addressed in transformative applications such as material handling, disaster response, casualty extraction, and personal assistance. Several configurations systems including single DOF aerial grasping, non-redundant articulated aerial manipulation, and fully-redundant articulated aerial manipulation have been explored to create manipulation systems [5]-[8].

All the arms in aerial manipulation are serial; a motor in each joint results in a heavy arm. To the authors' best knowledge, the authors' lab has been the first to introduce a

978-1-5386-3025-9/18/$31.00 ©2018 IEEE

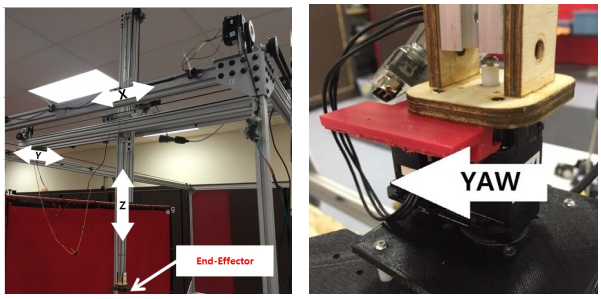

(a) End-effector Location and Height (b) End-effector Yaw movement

Fig. 3. The gantry crane system

parallel-mechanism arm for aerial manipulation [9]. Furthermore, there are few to no publications that highlight gripper designs for aerial manipulation. Given the precision needed for HTS micro-plate manipulation, sensorized grippers will be needed.

III. Hardware and Software Design

A. Mobility

To emulate rotorcraft drone motions, the 4-DOF gantry in Fig. 3 was employed [10]. The gantry's

$$1.2m \times 2.5m \times 0.5m$$

workspace has the footprint to emulate a small HTS or a section of a larger HTS. The gantry employs Dynamixel motors to provide end-effector cartesianal (x, y, z) position and yaw ψ orientation. The parallel-mechanism arm and gripper attach to the gantry's end-effector.

B. Parallel-Mechanism Manipulator

TABLE I
Physical Properties of the Manipulator Concept Design

Symbol	Value	Description
D_1	0.168 m	Fixed length link (base joint and knee)
D_2	0.216 m	Fixed length link (knee and top platform joint)
$L_(1,4,5,8)$	0.124 m	Length (origin to the base attachment point)
$L_(2,3,6,7)$	0.135 m	Length (origin to the base attachment point)
M_{tm}	0.682 kg	Total mass of manipulator concept design
M_{mm}	0.234 kg	Total mass of moving components

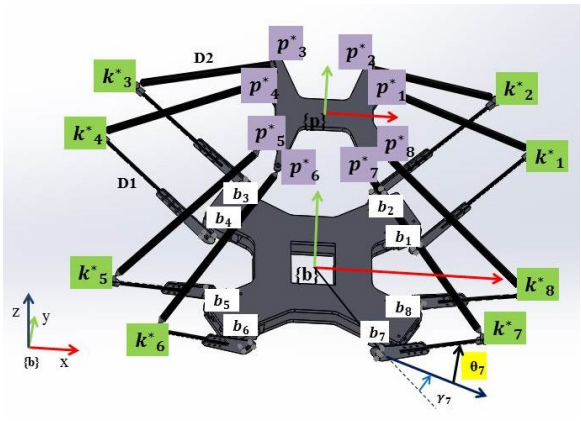

(a) CAD Design of the manipulator

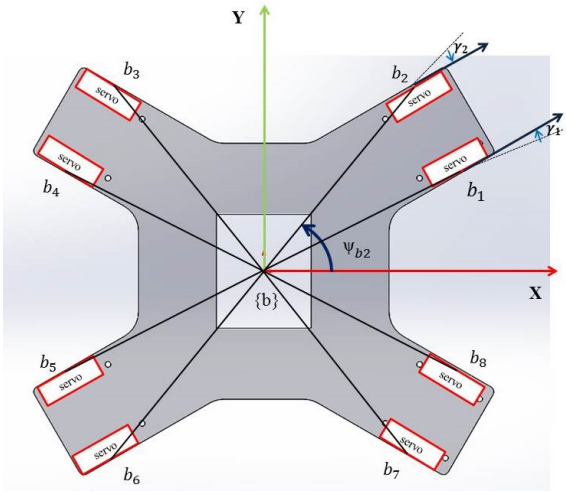

(b) Geometrical arrangement of leg attachment points

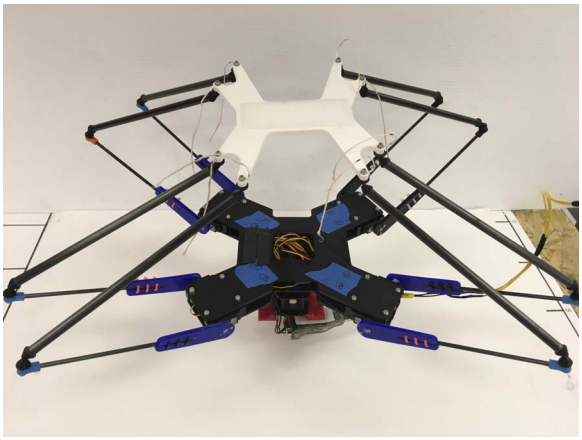

(c) Actual Design of the manipulator

Fig. 4. Parallel manipulator concept design (inverted for clarity)

A 6-DOF parallel-mechanism was selected to control micro-plate positioning and orientation because of its higher degree of precision versus serial manipulators [11], as shown in [9]. In Fig. 4, the manipulator was designed with 8 legs attaching the base b to a moving platform p. Each leg has one driven revolute joint and two spherical joints (8-RSS). All 8 motors work together to move the mass of the legs and the moving platform. Each leg, i, is attached to a servo on the base by a revolute joint. The servo drives a fixed length link, D_1, to an angle θ_i from the plane of the base. The D_1 link is connected to a second fixed length link, D_2, via a spherical "knee" joint, and the other end of the D_2 link attaches to the platform via

TABLE II
ANGULAR COORDINATES OF LEG ATTACHMENT POINTS TO THE BASE AND MOVING PLATFORM

Leg(i)	$\psi_{bi}(radians)$	$\gamma_i(radians)$	$\psi_{pi}(radians)$
1	0.3740	0.1496	0.5800
2	0.9622	0.4386	0.9753
3	2.1792	0.4388	2.1661
4	2.7674	0.1494	2.5614
5	3.5156	0.1496	3.7216
6	4.1038	0.4386	4.1169
7	5.3208	0.4388	5.3077
8	5.9090	0.1494	5.7030

TABLE III
LEG ATTACHMENT POSITIONS TO THE TOP AND BASE IN MANIPULATOR BASE COORDINATES

	Base Connections			Top Connections		
Leg(i)	$b_{xi}(m)$	$b_{yi}(m)$	$b_{zi}(m)$	$p_{xi}(m)$	$p_{yi}(m)$	$p_{zi}(m)$
1	0.1151	0.0451	0	0.0725	0.0475	0
2	0.0772	0.1108	0	0.0525	0.0775	0
3	-0.0772	0.1108	0	-0.0525	0.0775	0
4	-0.1151	0.0452	0	-0.0725	0.0475	0
5	-0.1151	-0.0452	0	-0.0725	-0.0475	0
6	-0.0772	-0.1108	0	-0.0525	-0.0775	0
7	0.0772	-0.1108	0	0.0525	0.0775	0
8	0.1151	-0.0452	0	0.0725	0.0475	0

a second spherical joint. The relative mounting positions of each leg is described in terms of angles ψ_{bi} and ψ_{pi} in the xy plane. γ_i is an angle between ψ_{bi} and the position of the link on the xy base plane, D_1. Table II and III shows the coordinates of each leg attachment point. All motors on the manipulator are controlled by the C++ open-source software, Pololu Mastro Servo Controller.

C. Parallel-Mechanism Manipulator Inverse Kinematics

The purpose of inverse kinematics for this parallel manipulator is calculated to identify goal angles for each of the 8 driven revolute joints around the base platform that will drive the top platform to a desired pose in the manipulator's base coordinates. The work in [9] and [12] described RSS (Revolute-Spherical-Spherical) generalized stewart platform [13] inverse kinematics.

The homogeneous transform ${}^bT_p$ is used to map each leg's attachment point to the top platform, p_i, to its goal pose p_i^* in manipulator's base coordinates as shown in Eq. 1

$$p_i^* = p_i {}^bT_p \tag{1}$$

Next, the Euclidean distance L_i^* is calculated as the direct distance between b_i and p_i^* for each leg. L_i^* is a virtual leg, and it is the hypotenuse of the triangle formed by the points b_i, p_i^* and the knee, m_i^*.

$$L_i^* = ||p_i^* - b_i|| \tag{2}$$

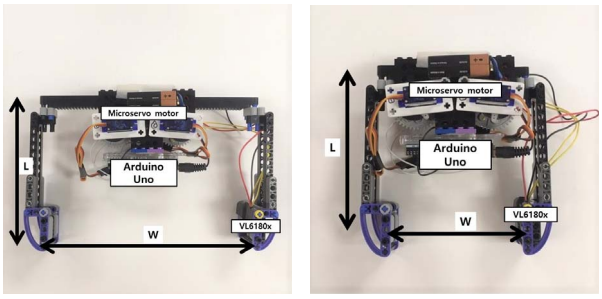

(a) Before gripping (b) After Gripping

Fig. 5. LEGO-Based parellel gripper concept design

Finally, the desired angle of servo rotation, θ_i, is calculated by Eq. 3

$$\theta_i = \arcsin(\frac{c}{\sqrt{a^2+b^2}}) - \arctan(\frac{b}{a}), \tag{3}$$

where:

$a = 2D_1(p_{zi}^* - b_{zi})$

$b = 2D_1[(p_{xi}^* - b_{xi})\cos(\psi_{bi} \pm \gamma_i) + (p_{yi}^* - b_{yi})\sin(\psi_{bi} \pm \gamma_i)]$

$c = L_i^{*2} - D_2^2 + D_1^2$.

In b, the sum of the angles is used in the sinusoids for legs L_2, L_4, L_6, and L_8, while the difference of the angles is used for legs L_1, L_3, L_5, and L_7.

D. LEGO-Base Sensorized Parellel Jaw Gripper

TABLE IV
PHYSICAL PROPERTIES OF THE GRIPPER CONCEPT DESIGN

Symbol	Value	Description [m]
W	0.095-0.195m	Width between grip and non-grip
H	0.15 m	Height of the gripper
M_{tg}	0.297 kg	Total mass of the gripper concept design

For rapid prototyping, LEGO was used to construct the sensorized parallel jaw gripper for grasping work.(See Fig 5). The gripper is operated by servomotors that react to tactile feedback from an inter-integrated-circuit(I^2C) compatible time of flight(ToF) sensor, VL6180X (STMicroelectronics). The sensor is mounted right bottom side of the gripper in-hand. An I^2C compatible Arduino-Uno is used to operate the gripper and receive proximity range data from the sensor. The grasping begins when the object contacts the gripper. The gripper is mounted under the platform of the parallel manipulator. The application of this low cost in-hand sensing gripper for aerial grasping is novel. Barriers to their use include cost, difficulty of manufacture, and the scarcity of algorithms for reactive grasp planning. This was illustrated in the 2015 Amazon Picking Challenge [14].

E. Parallel-Mechanism Manipulator and Gripper Design Criteria

Several factors were considered while designing the parallel-mechanism manipulator and gripper (PMG). The Tarot

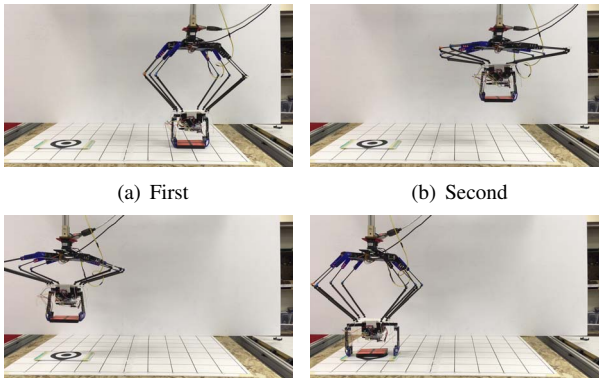

(a) First (b) Second

(c) Third (d) Fourth

Fig. 6. Expereiment procedure

X6 hexacopter was selected to fly the manipulator, so the thrust of the drone should be able to support the weight of the PMG and micro-plate load. The payload of the Tarot X6 is estimated to be $8.8kg$ [15]. Therefore the target weight of the PMG is $2kg$ considering the weights of other components(battery, frame, and etc) or less. In addition, it is important to minimize torque on the UAV from the manipulator. The parallel manipulation mechanism presented was selected because it allows all motors to be mounted rigidly. Therefore the manipulator impact on the UAV's stability is minimized. The final design of PMG is composed of a manipulator and a gripper with a total mass of $0.979kg$ and a moving mass of $0.531kg$

The shape of the tarot x6 hexacopter further informed manipulator design. The position of each leg on the base platform, ψ_{bi} and γ_i, were selected to ensure that the manipulator's legs do not contact the hexacopter's landing gears while stowed and deployed.

Furthermore, it would be desirable to allow the manipulator to lay against the base. This would facilitate grasping work within the limited workspace under the hexacopter ($40cm$ high). To enable this, the relationship between D_1 and D_2 was calculated in Eq. 4

$$D_1 = ||k_i^* - b_i||, \tag{4}$$

where:

$$k_i^* = \begin{bmatrix} k_{xi}^* \\ k_{yi}^* \\ k_{zi}^* \end{bmatrix} = \begin{bmatrix} D_1 \cos(\psi_{bi} \pm \gamma_i)\cos(\theta_i) + b_{xi} \\ D_1 \sin(\psi_{bi} \pm \gamma_i)\cos(\theta_i) + b_{yi} \\ D_1 \sin(\theta_i) + b_{zi} \end{bmatrix} \tag{5}$$

with θ_i = 0.

In designing the gripper, space for an arduino uno and the lego servomotors was considered as short as it could be. Therefore the gripper height was selected to be $15cm$. Grasping range is determined by the size of a micro-plate. The physical properties of the gripper are listed in Table IV These components were mounted to the platform of the parallel manipulator.

IV. Experimental Results

For testing, the PMG was affixed to a gantry system. A $90cm$ x $140cm$ rectangular coordinate system was positioned below the PMG to measure the accuracy of linear translations. Angular translations were measured against a protractor. A micro-plate prototype was constructed from dimensions in [16] with a black cross to mark the center.

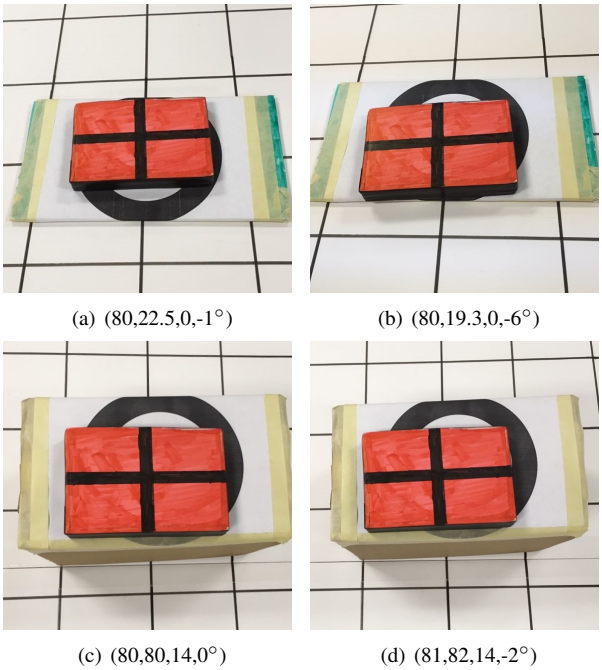

(a) (80,22.5,0,-1°) (b) (80,19.3,0,-6°)

(c) (80,80,14,0°) (d) (81,82,14,-2°)

Fig. 7. Linear translation experiment result

Each test included four steps. First, the PMG descends $20cm$ and grasps the micro-plate. Second, PMG returns to its initial position. Third, the gantry system moves the PMG to the target location. Finally, the manipulator lowers the gripper to the target location and the gripper releases the micro-plate. (See Figure. 6)

Table V describes the final rotation angle of the revolute joint on each leg during the experiments, calculated from Eq. 3. Figure. 7 shows the results of the linear translation experiment. The micro-plate was placed at an initial position of s=(20, 20, 0, 0°). (a) and (b) show the results of transportation to the target location of (80, 80, 0, 0°), and (c) and (d) show the

TABLE V
Rotation angle of revolute joint from experiments

Positions			
Store and Delivery		Pick-up	
Joint(i)	$\theta_i(radians)$	Joint(i)	$\theta_i(radians)$
1	0.0252	1	0.5302
2	0.0536	2	0.5614
3	0.0536	3	0.5614
4	0.0252	4	0.5302
5	0.0248	5	0.5302
6	0.0536	6	0.5614
7	0.0537	7	0.5614
8	0.0252	8	0.5302

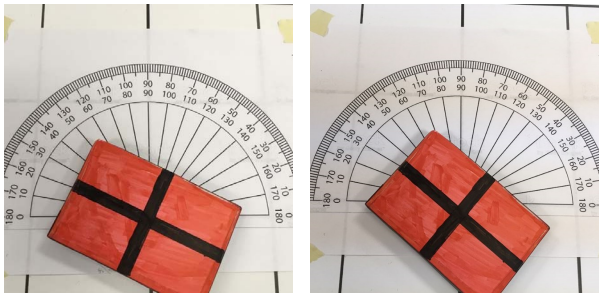

(a) Rotates to 30° (27.8°)

(b) Rotates to 45° (40°)

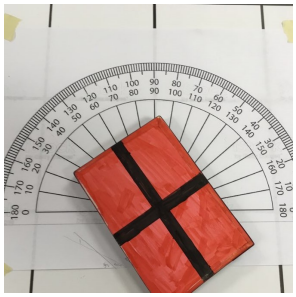

(c) Rotates to 60° (57.2°)

(d) Rotates to 90° (86.5°)

Fig. 8. Angular translation experiment result

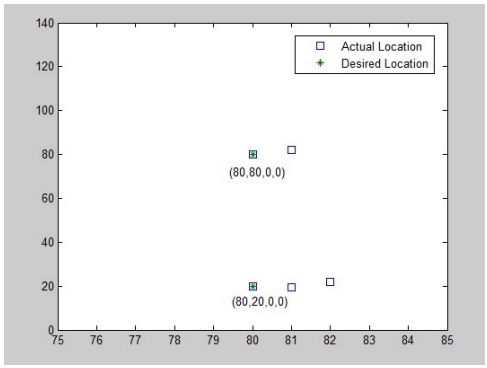

(a) Linear translation experiment result

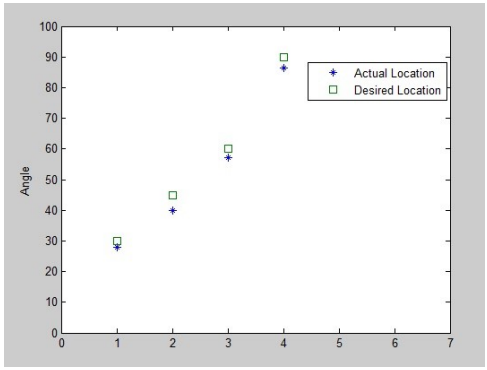

(b) Angular translation experiment result

Fig. 9. Error between desired location and actual location

results of transportation to (80, 80, 14, 0°). Figure. 8 shows the results of the angular translation tests in which the PMG is set to rotate the micro-plate by 30, 45, 60, 90 degrees respectively. The dot graph in Figure. 9 shows the error between target position and actual position. The linear translation experiment resulted in an average of 1.25 percent error in x direction translation and 4 percent error in y direction translation. The average error for angular translation trials was 6.75 percent.

V. Conclusion and Future Work

In this paper, a 6 DOF parallel mechanism manipulator with a sensorized parallel jaw gripper was designed for lab automation drone in high throughput systems. A 4 degree of freedom gantry crane was utilized to emulate UAV motions in a HTS workspace. The experimental results show the design facilitates micro-plate positioning and orienting with a high degree of precision.

Future work will consist of more testing and evaluation. The performance and design of the manipulator and sensorized jaw gripper will be updated. Then, the improved design will be mounted on a UAV and deployed inside a mock HTS environment for more variable grasping tasks.

References

[1] Sneader, Walter (1985) Drug Discovery: The Evolution of Modern Medicines. John Wiley and Sons, New York, NY

[2] William P. Janzen (2002) High Throughput Screening : Methods and Protocols. Humana Press

[3] Tecan Robotic Arms[Online]
Available : http://lifesciences.tecan.com/products/

[4] RX160 6-axis industrial robot, STAUBLI[Online]
Available : https://www.staubli.com/en/robotics/6-axis-scara-industrial-robot/medium-payload-6-axis-robot/6-axis-industrial-robot-rx160/

[5] Q. Lindsey, D.Mellinger, and V. Kumar, "Construction of cubic structures with quadrotor teams," Proc. Robotics: Science and Systems VII, 2011

[6] M. Orsag, C. Korpela, S. Bogdan, and P.Oh, "Valve turning using a dual-arm aerial manipulator," in Unmanned Aircraft Systems(ICUAS), 2014 International Conference on. IEEE, 2014, Pp. 836-841

[7] T. W. Danko and P.Y. Oh, "Design and control of a hyper-redundant manipulator for mobile manipulating unmanned aerial vehicles," Journal of Intelligent and Robotics Systems, PP. 1-15, 2013

[8] D. Mellinger, Q. Lindsey, M. Shomin, and V. Kumar, "Design, modeling, estimation and control for aerial grasping and manipulation," in Intelligent Robots and Systems(IROS), 2011 IEEE/RSJ International Conference on. IEEE, 2011, pp. 2668-2673

[9] T. W. Danko, K. P. Chaney, and Paul Y. Oh, "A Parellel Manipulator for Mobile Manipulating UAVs," Technologies for Practical Robot Applications (TePRA), 2015 IEEE International Conference on. IEEE 2015, pp.1-6

[10] C. Korpela, T. W. Danko, and Paul Y. Oh, "Designing a System for Mobile Manipulation from an Unmanned Aerial Vehicle," Technologies for Practical Robot Applications (TePRA), 2011 IEEE Conference on. IEEE, 2011, pp. 109-114

[11] T. W. Danko, and Paul Y. Oh, "Evaluation of visual servoing control of aerial manipulators using test gantry emulation,"in Unmanned Aircraft Systems(ICUAS), 2014 International Conference on. IEEE, 2014, pp. 821-829

[12] F. Szufnarowski, "Stewart platform with fixed rotary actuators a low cost design study," Advances in Medical Robotics, 2013

[13] D. Stewart, "A platform with six degrees of freedom," proceedings of the institution of mechanical engineers. vol. 180, no. 1. pp. 371-386, 1965

[14] Nikolaus Correll, Kostas E. Bekris, Dmitry Berenson, Oliver Brock, Albert Causo, Kris Hauser, Kei Okada, Alberto Rodriguez, Joseph M. Romano, and Peter R. Wurman, "Lessons from the Amazon Picking Challenge," arXiv:1601.05484, 2016

[15] J. Sedden, Ph.D. (1990), Basic Helicopter Aerodynamics

[16] Technical Data Sheet 96-Well English Cell Culture Plate, Eppendorf[Online]
Available : https://online-shop.eppendorf.com/OC-en/eshopdownload/